Available online at www.sciencedirect.com
ScienceDirect
Journal of Solid State Chemistry 179 (2006) 3484–3488
JOURNAL OF SOLID STATE CHEMISTRY
www.elsevier.com/locate/jssc

# The mixed valent tellurate $SrTe_3O_8$: Electronic lone pair effect of $Te^{4+}$

N. Barrier[a,*], S. Malo[a], O. Hernandez[b], M. Hervieu[a], B. Raveau[a]

[a]*Laboratoire CRISMAT, UMR 6508 CNRS Ensicaen, 6 bd Maréchal Juin, 14050 Caen Cedex 4, France*
[b]*UMR 6226 CNRS-Université de Rennes 1 Sciences Chimiques de Rennes, Equipe Matériaux inorganiques: chimie douce et réactivité, Bât. 10B, campus de Beaulieu, 263, avenue du Général Leclerc, F-35042 Rennes, France*

Received 14 April 2006; received in revised form 30 June 2006; accepted 7 July 2006
Available online 16 July 2006

**Abstract**

A novel mixed valent tellurium oxide, $SrTe_3O_8$, has been synthesized and its crystal structure was determined ab initio from powder X-ray diffraction data. This oxide, which crystallizes in a tetragonal unit-cell, $P4_2/m$ space group, with very close $a$ and $c$ cell parameters (6.8257(1) and 6.7603(1) Å, respectively), exhibits a very original structure built up of corner-sharing $TeO_6$ ($Te^{6+}$) octahedra and $Te_2O_8$ ($Te^{4+}$) twin-pyramidal units. The latter ones form $[Te_3O_8]_\infty$ chains running along the [001] and the [110] directions. Besides the four sided tunnels where the $Sr^{2+}$ cations are located, there are very large four sided tunnels running along the $c$-axis which are obstructed by the electronic lone pairs of the $Te^{4+}$ cations.


*Keywords:* Mixed valent tellurium oxide; Synthesis; Tunnel structure; Electron microscopy; X-ray powder diffraction; Ab initio structure determination; Rietveld refinement; Electronic lone pairs

## 1. Introduction

The chemistry of tellurium oxides is mainly governed by the existence of two oxidation states for tellurium: $Te^{6+}$ and $Te^{4+}$. In spite of their very different stereochemical behaviour, these two species were currently observed to coexist in the same structure. It is the case, for example of the mixed valent oxides $Te_2O_5$ and $Te_4O_9$ [1,2] and of the ternary oxides $K_2Te_4O_{12}$ [3] and $BaTe_2O_6$ [4].

Among the various ternary oxides, the Sr–Te–O system shows rather rich crystal chemistry: on the one hand, Te(VI) oxide compounds such as $SrTeO_4$ [5,6], exhibit $Te^{6+}$ cations with an octahedral coordination and on the other hand, Te(IV) oxides such as $SrTeO_3$ [7–9], $SrTe_5O_{11}$ [10] and $Sr_3Te_4O_{11}$ [11] show $Te^{4+}$ cations with several different environments due to the strong stereoactivity of its electronic lone pair. A few Te(IV)-based compounds, $SrTe_2O_5$ [12–14], $Sr_2Te_3O_8$ [15], and of Te(VI), $Sr_3TeO_6$ [16] have been reported but no structures have been determined. A better understanding of stereochemical behaviour of tellurium needs an acute investigation of this system. We report herein the synthesis and the crystal structure, determined ab initio using powder X-ray diffraction data, of a novel mixed valent tellurium oxide $SrTe_3O_8$, with an original tunnel structure. This compound shows perfectly ordered $Te^{4+}$ and $Te^{6+}$ species that form cross-linking chains of $TeO_5E$ and $TeO_6$ octahedra, respectively, $E$ representing the electronic lone pair of $Te^{4+}$.

## 2. Experimental section

### 2.1. Synthesis

The $SrTe_3O_8$ oxide was synthesized by solid state reaction from a stoichiometric mixture of $SrO_2$ (Acros; 99% stored in glove box under Ar atmosphere) and $TeO_2$ oxides (Alfa aesar; 99,99%). The samples were first intimately ground in an agate mortar then pressed in the form of bars. They were placed in evacuated quartz tubes and heated up to 650 °C with a heating rate of 100 °C $h^{-1}$, held at this temperature for 12 h and cooled to room temperature in 6 h.

*Corresponding author. Fax: +33 2 31 95 16 00.
*E-mail address:* nicolas.barrier@ensicaen.fr (N. Barrier).

0022-4596/$ - see front matter © 2006 Elsevier Inc. All rights reserved.
doi:10.1016/j.jssc.2006.07.012

### 2.2. Electron microscopy

The electron diffraction (ED) study was carried out with a JEOL 200CX electron microscope fitted with an eucentric goniometer ($\pm 60^\circ$) equipped with an energy dispersive spectroscopy (EDS) analyzer. For the transmission electron microscopy study, the samples were crushed in alcohol and deposited on a holey carbon membrane supported by a copper grid.

### 2.3. Powder X-ray diffraction

Powder X-ray diffraction patterns were collected with two $\theta$–$\theta$ para focusing Bragg–Brentano geometry diffractometers. For the first time the data collection was performed on a high-resolution Bruker AXS D8 Advance using pure Cu$K\alpha_1$ radiation (1.54056 Å), selected by an incident beam Ge Johannson monochromator, equiped with a receiving slit of 0.1 mm and a Sol-X detector, in the angular range $16^\circ < 2\theta < 133^\circ 2\theta$. Data were collected using a various step scan: $0.007^\circ 2\theta$/step ranging from $16^\circ$ to $77^\circ 2\theta$; $0.010^\circ 2\theta$/step ranging from $77^\circ$ to $113^\circ 2\theta$; $0.015^\circ 2\theta$/step ranging from $113^\circ$ to $133^\circ 2\theta$ and were normalized to a constant acquisition time of 18.93 s. A second set of data was recorded with a PANalytical X'pertPro diffractometer equipped with an X'Celerator detector working with the Cu$K\overline{\alpha}$ radiation (1.54184 Å) in the $2\theta$ range 10–150° (Table 1). Both data collections were performed at room temperature with back-loading sample holders to avoid preferred orientation of crystallites and were then analysed by whole-powder-diffraction-pattern profile refinement with the Jana2000 program [17].

Table 1
Conditions of X-ray data collection and agreement factors for $SrTe_3O_8$

| | |
|---|---|
| Diffractometer | Philips X-pert Pro |
| Angular range ($^\circ 2\theta$) | 10–150 |
| Step size ($^\circ 2\theta$) | 0.0040 |
| Scan step time (s) | 301.35 |
| PSD mode-length ($^\circ 2\theta$) | Scanning—2,12 |
| Measurement temperature (°C) | 25.00 |
| Radiation type | Cu$K\overline{\alpha}$ (1.54184 Å) |
| Number of points | 34,999 |
| Total number of refined parameters | 22 |
| Number of reflections | 352 |
| Number of refined crystallographic parameters | 16 |
| Profile function | Thompson–Cox–Hastings pseudo-Voigt |
| Background function | Manual background |
| Asymmetry correction | by divergence (Finger, Cox and Jephcoat) |
| Preferred orientation | March and Dollase |
| $R_{obs}$ | 0.0452 |
| $R_p$ | 0.0465 |
| $R_{wp}$ | 0.0590 |
| $R_{exp}$ | 0.0392 |

### 2.4. Crystal structure determination

The electron diffraction characterization was carried out at room temperature. The reciprocal space was reconstructed by tilting around the different axes. The ED patterns of $SrTe_3O_8$ recorded along [001] and [0$\bar{1}$1] are given as examples in Fig. 1. They evidence that the cell parameters are $a \approx b \approx c \approx 6.8$ Å without any condition limiting the reflection. The cationic composition determined by EDS analyses on numerous crystallites is similar to the nominal composition. The amorphization of the sample under the electron radiation did not allow us to perform a high-resolution electron microscopy study.

For the automatic indexing procedure as well as for the extraction of the structure factor moduli, the first set of high-resolution powder XRD data recorded with pure Cu$K\alpha_1$ radiation on the D8 Advance diffractometer (Fig. 2), was considered to limit peak overlaps, in order to obtain very accurate peak positions and structure factor moduli.

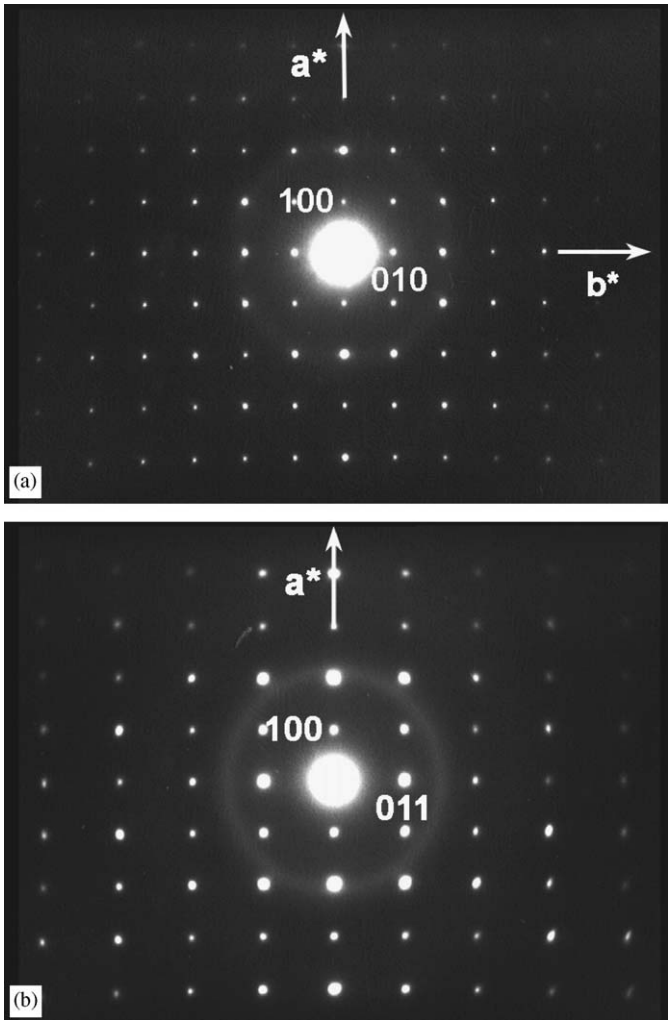


Fig. 1. Electron diffraction patterns of $SrTe_3O_8$ recorded along (a) [001] and (b) [0$\bar{1}$1] zone axes.

A careful observation of this X-ray pattern shows the presence of few impurities corresponding to the $SrTe_2O_5$ phases [12–14]. The WinPLOTR programme [18] was used for the peak position calculation and the automatic indexation was carried out with the DICVOL04 programme [19] against the first 21 experimental diffraction peaks. A tetragonal solution was found with very close $a = 6.8241(1)$ Å and $c = 6.7589(2)$ Å unit-cell parameters with the following figures of merit: $M_{20} = 372.1$; $F_{20} = 396.3(0.0016, 31)$. Whole X-ray powder pattern refinement with cell constraint was then performed in this tetragonal unit cell with $P4$ space group, which presents no conditions limiting possible reflections. A meticulous examination of the indexed pattern shows that all $0\,0\,l$ reflections with $l = 2n+1$ are missing. This condition is consistent with the $P4_2$, $P4_2/m$ and $P4_222$ space groups. The extraction of the structure factor moduli using the Le Bail method was carried out with the Jana2000 program [17] and direct method procedures were then performed with the Expo program [20] for these three space groups. The best solution was obtained for the $P4_2/m$ space group with a quite good reliability factor $R_F = 7.70\%$ and all the crystallographic positions of the Sr, Te and O atoms were directly found. Rietveld refinements of this model give a good structure factor $R_{obs} = 6.32\%$ and profile factors ($R_p = 18.77\%$; $R_{wp} = 27.59\%$; gof = 1.24). Nevertheless some isotropic atomic displacements parameters were nonpositive definite. Thus another XRD data set was then recorded on a Panalytical X'pert pro diffractometer ($CuK\overline{\alpha}$) equipped with an X'celerator detector to improve the counting statistics. Refinements of all profile and structural parameters yield to the following reliability factors: $R_{obs} = 4.52\%$; $R_p = 4.65$; $R_{wp} = 5.90$; $R_{exp} = 3.92$; gof = 1.51 with all the isotropic atomic displacement parameters positive defined. The comparison between observed and the calculated pattern and the difference curve are shown in Fig. 2. The presence of the $SrTe_2O_5$ phases were not taken into account in the refinement since their crystal structures are not yet been solved. The refinement conditions and the crystallographic parameters with selected bond distances are given in the Tables 1 and 2,

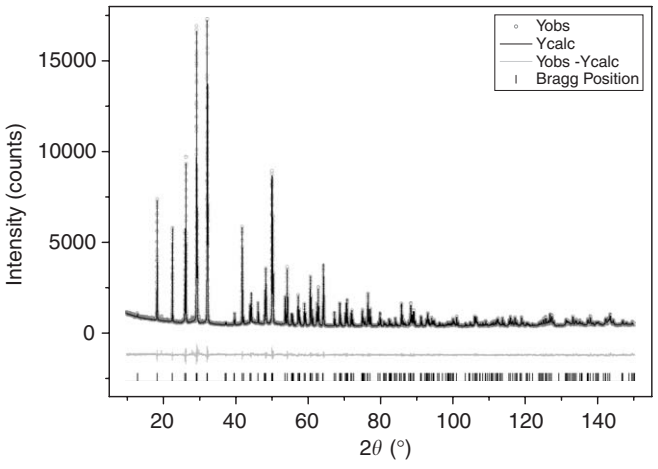


Fig. 2. X-ray powder diffraction pattern of $SrTe_3O_8$, PANalytical X'pertPro diffractometer $CuK\overline{\alpha}$ radiation (1.54184 Å), with observed (dots), calculated (solid line), Bragg reflections (ticks) and difference profiles.

Table 2
Crystallographic parameters of $SrTe_3O_8$

| Crystal data | |
|---|---|
| Formula sum | $O_8\ Sr_1\ Te_3$ |
| Crystal system | Tetragonal |
| Space group | $P42/m$ (no. 84) |
| Unit cell dimensions | $a = 6.8257(1)$ Å |
| | $c = 6.7603(1)$ Å |
| Cell volume | 314.966(4) Å$^3$ |
| $Z$ | 2 |

Atomic coordinates and isotropic displacement parameters (in Å$^2$)

| Atom | Wyck. | Sym. | $x$ | $y$ | $z$ | $U_{iso}$ |
|---|---|---|---|---|---|---|
| Te1 | 4*j* | *m*.. | 0.06251(8) | −0.28185(8) | 1/2 | 0.0070(1) |
| Te2 | 2*d* | 2/*m*.. | 1/2 | 0 | 1/2 | 0.0073(2) |
| Sr | 2*e* | −4.. | 1/2 | −1/2 | 1/4 | 0.0150(3) |
| O1 | 4*j* | *m*.. | 0.3854(6) | −0.2549(8) | 1/2 | 0.0026(13) |
| O2 | 4*j* | *m*.. | 0.8189(6) | −0.4636(7) | 1/2 | 0.0052(13) |
| O3 | 8*k* | 1 | 0.0926(5) | −0.3143(5) | 0.1952(4) | 0.0046(9) |

Interatomic distances (in Å)

| | | | |
|---|---|---|---|
| Te1–O1 | 2.211(4) × 1 | Te2–O1 | 1.908(5) × 2 |
| Te1–O2 | 2.075(4) × 1 | Te2–O3 | 1.936(3) × 4 |
| Te1–O2 | 1.917(4) × 1 | Sr1–O1 | 2.503(4) × 4 |
| Te1–O3 | 2.083(3) × 2 | Sr1–O2 | 2.767(3) × 4 |

respectively. Further details of the crystal structure investigation can be obtained from the Fachinformationszentrum Karlsruhe, 76344 Eggenstein-Leopoldshafen, Germany (fax: +49-7247-808-666; e-mail: crysdata@fiz.karlsruhe.de) on quoting the depository number CSD 416448.

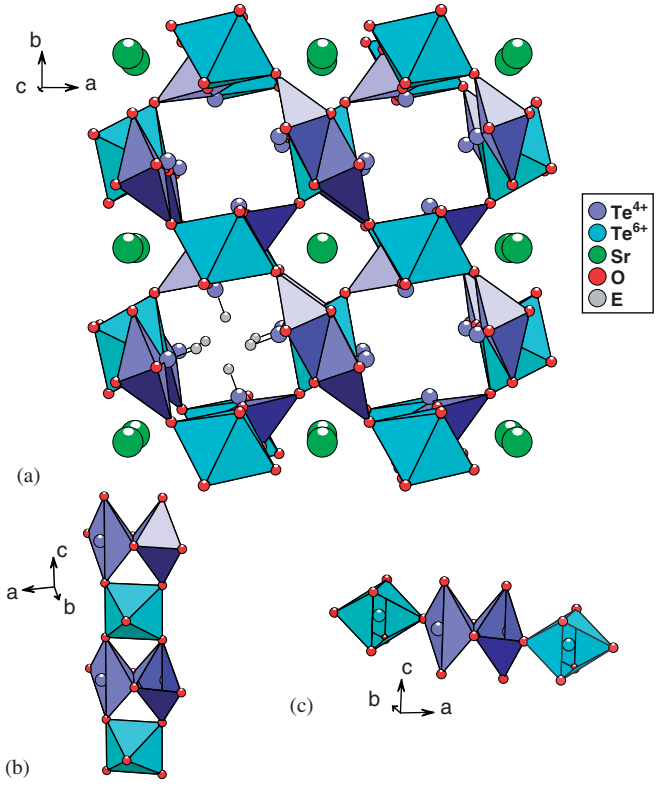


Fig. 3. (a) Structure of $SrTe_3O_8$ along the *c*-axis, showing two types of square base tunnels: the smallest ones occupied by $Sr^{2+}$ cations and largest ones obstructed by the $Te^{4+}$ lone pairs. (b) $[Te_3O_8]_\infty$ unit chain running along the *c*-axis build up of $TeO_6$ octahedra and two trans-edge sharing $TeO_5$ square base pyramids ($Te_2O_8$ unit). (c) $TeO_6$ octahedra alternate with $Te_2O_8$ twin-pyramids to form $[Te_3O_8]_\infty$ unit chain parallel to the [110] direction.

## 3. Description of the structure and discussion

The projection of the tunnel structure of this new phase along the *c*-axis is shown in Fig. 3a. The Diamond *ver* 3.0 program was used for structure visualization. [21] The structure can be described from a $[Te_3O_8]$ framework built up from $TeO_6$ octahedra sharing corners with two $TeO_5$ square base pyramids that share one edge to form twin-pyramid units $Te_2O_8$. Along the *c*-axis (Fig. 3b), $TeO_6$ octahedra alternate with $Te_2O_8$ twin-pyramids. One $TeO_6$ octahedron shares its square base corners with the apices of two $Te_2O_8$ twin-pyramids to form $[Te_3O_8]_\infty$ infinite chains running along the *c*-axis. Fig. 3c also shows that similarly $Te_2O_8$ twin-pyramids can be alternatively assembled with $TeO_6$ octahedra through their corners to obtain $[Te_3O_8]_\infty$ infinite chains running along the [110] direction. By this way, the entire framework can be described from the assemblage of these [110] $[Te_3O_8]_\infty$ infinite chains. Moreover, the chains running along a same direction, e.g. [110], are interconnected through identical chains oriented at 90°, i.e. along [1–10] and located above and below them along the *c*-axis. Note that in this framework, each $TeO_6$ octahedron is linked to four $Te_2O_8$ twin-pyramids and reciprocally the latter ones are linked individually to four $TeO_6$ octahedra.

The projection along the *c*-axis (Fig. 3) also shows square tunnels running along that direction. Two sorts of tunnels can be distinguished: the smaller ones which are occupied by strontium, whereas the larger ones are apparently empty. In fact, the tellurium cations belonging to the pyramids (labelled Te1) are off-centred toward the tunnel axis so that this geometry, often observed for lone pair cations, can be attributed to $Te^{4+}$. According to the VSEPR theory, [22,23] the Te1 atoms exhibit an octahedral $TeO_5E$ geometry, the electronic lone pair *E* sitting at an apical position, inside the large tunnels. Thus, we can consider that these large tunnels are obstructed by the electronic lone pairs which behave as anions: two lone pairs belonging to opposite walls are located at the same level along *c*-axis.

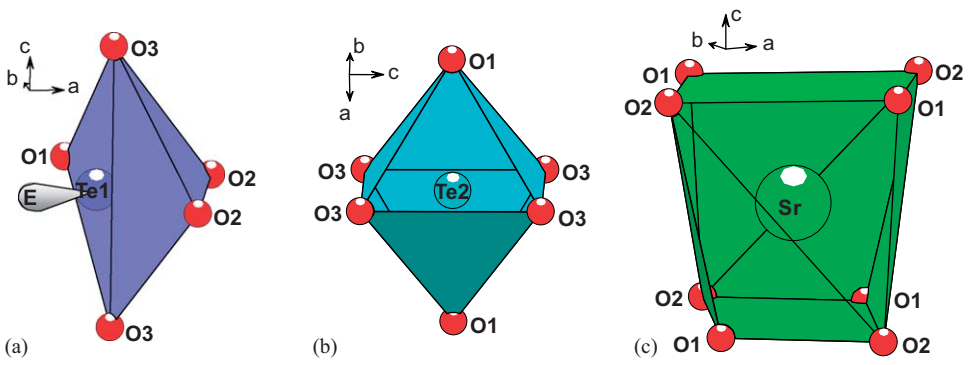


Fig. 4. Oxygen environment of the tellurium and strontium cations in $SrTe_3O_8$: (a) octahedral coordination ($TeO_5E$) of the Te1 atom type, (b) octahedral coordination ($TeO_6$) of the $Te_2$ atom type and (c) 8-fold coordination of the Sr atom type.

The 1/2 ordering of the $Te^{6+}/Te^{4+}$ species is strongly supported by the interatomic distances observed for the polyhedra (Table 2). The $TeO_5E$ octahedron (Fig. 4a) is distorted with an apical Te1–O2 distance of 1.917(4) Å shorter than the four other equatorial ones which are ranging from 2.075(4) to 2.211(4) Å. These features, as well as the off-centring of the $Te^{4+}$ cation, confirm the stereochemical activity of the lone pair. Assuming the method given by Galy et al. [24] the empirical localization of the electronic lone pair in the structure (Fig. 4a) was performed: first the position of the centre of mass $G$ of the basal plan of the octahedron built up of the O1, O3, O2, O3 atoms (Fig. 4a) is determined, then the position of $E$ is calculated by extending the [O2$G$] segment, between the apical O2 atom and $G$, of an equivalent distance with $O2G = GE$. The coordinates of $E$ are $x = 0.8625$; $y = 0.986$; $z = 0$ and the Te1–$E$ distance is 1.04 Å. This value is rather short compared to the average one of 1.25 Å calculated by Galy et al. [24] as well as those calculated for the same $TeO_5E$ environment in $BaTe_2O_6$ [4] and $K_2Te_4O_{12}$ [3], respectively 1.34 and 1.38 Å. Such very short Te–$E$ distance is observed in the $Te_2O_5$ compound [1] in which $Te^{4+}$ adopts a $TeO_4E$ environment with a Te–$E$ distance of 1.02 Å. In our case, the reduction of the Te1–$E$ distance can be explained by the necessity to limit the electronic repulsions. For two lone pairs located at the same level along the $c$-axis within the largest tunnel of 3.93 Å width, the $E$–$E$ distance is indeed close to 1.89 Å. The octahedral environment of the $Te^{6+}$ cation (Fig. 5b) is much more regular with two apical Te2–O1 distances of 1.908(5) Å and four equatorial Te2–O3 distances of 1.936(3) Å. Bond valence sum calculations [25,26] confirm the presumed oxidation state of Te1 and Te2 with valency values of 3.95(2) and 5.69(3), respectively.

The $Sr^{2+}$ cations are in eight-fold coordination environments (Fig. 5c) with Sr–O distances ranging from 2.503(4) to 2.767(3) Å and bond valence sum calculations give a value of 2.11(3).

## 4. Conclusion

A new mixed valent tellurium oxide with an original tunnel structure has been synthesized and its crystal structure determined ab initio using powder X-ray diffraction data. In this structure the $Te^{6+}$ and $Te^{4+}$ species are ordered and form a three-dimensional framework. Two trans-edge sharing $TeO_5$ square base pyramids ($Te^{4+}$) form a twin-pyramid unit $Te_2O_8$ and alternate with $TeO_6$ octahedra ($Te^{6+}$) along the three directions. These results suggest that in spite of the numerous investigations carried out in this field, many mixed valent tellurium oxides remain to be discovered, due to the great ability of $Te^{4+}$ and $Te^{6+}$ to accommodate various structural distortions.

## References

[1] O. Lindqvist, J. Moret, Acta Crystallogr. B 29 (1973) 643.
[2] O. Lindqvist, W. Mark, J. Moret, Acta Crystallogr. B 31 (1975) 1255.
[3] F. Daniel, J. Moret, M. Maurin, E. Philippot, Acta Crystallogr. B 34 (1978) 1782.
[4] M. von Koçak, C. Platte, M. Trömel, Acta Crystallogr. B 35 (1979) 1439.
[5] D. Hottentot, B.O. Loopstra, Acta Crystallogr. B 35 (1979) 728.
[6] J. Lapasset, J. Moret, Acta Crystallogr. C 41 (1985) 1558.
[7] I. Ismailzade, Phys. Stat. Sol. A 52 (1979) K105.
[8] Y. Elerman, Doga, Turk. J. Phys. 17 (1993) 465.
[9] H.G. Burckhardt, M. Koçak, N. Külcü, M. Trömel, J. Solid State Chem. 54 (1984) 256.
[10] H. Burckhardt, M. Tromel, Acta Crystallogr. C 39 (1983) 1322.
[11] O.A. Dytyatyev, V.A. Dolgikh, Mater. Res. Bull. 34 (1999) 733.
[12] M. Redman, et al., J. Am. Ceram. Soc. 53 (1970) 645.
[13] S. Malyutkin, et al., Russ. J. Inorg. Chem. (1971) 16916.
[14] M. Trömel, H. Ziethen-Reichnach, Z. Anorg. Allg. Chem. 378 (1970) 232.
[15] Y. Elerman, M. Kocak, J. Appl. Crystallogr. 19 (1986) 410.
[16] M. Trömel, 1984, private communication.
[17] V. Petricek, et al., JANA2000 software, Institute of Physics Academy of Sciences of the Czech Republik, Prague.
[18] T. Roisnel, J. Rodriguez-Carvajal, WinPLOTR: a windows toll for powder diffraction patterns analysis, in: Proceedings of the European Powder Diffraction Conference (EPDIC7), Mater. Sci. Forum 378 (2001) 118.
[19] A. Boultif, D. Louer, J. Appl. Crystallogr. 37 (2004) 724.
[20] A. Altomare, M.C. Burla, M. Camalli, B. Carrozzini, G. Cascarano, C. Giacovazzo, A. Guagliardi, A.G.G. Moliterni, G. Polidori, R. Rizzi, J. Appl. Crystallogr. 32 (1998) 339.
[21] K. Brandenburg, Diamond Version 3.0. Crystal Impact GbR, Bonn, Germany, 1999.
[22] R.J. Gillespie, R.S. Nyholm, Quart. Rev. 11 (1957) 339.
[23] R.J. Gillespie, Molecular Geometry, Van Nostrand Reihold, Londres, 1972.
[24] J. Galy, G. Meunier, S. Anderson, A. Åström, J. Solid State Chem. 13 (1975) 142.
[25] I.D. Brown, D. Altermatt, Acta Crystallogr. B 41 (1985) 244.
[26] N.E. Brese, M. O'Keeffe, Acta Crystallogr. B 47 (1991) 192.